Hindawi
Shock and Vibration
Volume 2022, Article ID 6808641, 9 pages
https://doi.org/10.1155/2022/6808641

Research Article

Single Feature Extraction Method of Bearing Fault Signals Based on Slope Entropy

Erna Shi

Xi'an Traffic Engineering Institute, Xi'an, Shaanxi 710300, China

Correspondence should be addressed to Erna Shi; shierna0719@163.com

Received 5 April 2022; Revised 22 April 2022; Accepted 6 May 2022; Published 2 June 2022

Academic Editor: Yuxing Li

As an entropy representing the complexity of sequence, slope entropy (SloE) is applied to feature extraction of bearing signal for the first time. With the advantage of slope entropy in feature extraction, the effectiveness of bearing fault signal diagnosis can be verified. Five different kinds of entropy are selected to be comparative methods for experiments, and they are permutation entropy (PE), dispersion entropy (DE), a version of entropy adapted by PE, which is weighted permutation entropy (WPE), and two versions of entropy adapted by DE, which are fluctuating dispersion entropy (FDE) and reverse dispersion entropy (RDE). A method of extracting a single feature of bearing fault signals based on SloE is carried out. Firstly, the features of the bearing signals are extracted by the six kinds of entropy. Then, some relevant data are computed, and the identification ratios are calculated by the K-nearest neighbor (KNN) algorithm. The experimental result indicated that the identification ratio of SloE is the highest at 97.71% by comparing with the identification ratios of the other five kinds of entropy, which is higher by at least 13.54% than the others and 27.5% higher than the lowest one.

1. Introduction

Bearing is an indispensable part of modern mechanical equipment, and its roles in modern mechanical equipment are the support of the mechanical rotating body, the sliding part in motion, and the guarantor of rotation accuracy [1–3]. Self-aligning ball bearing is the research object of this paper, which is a kind of rolling bearing equipped with spherical balls installed between the inner race with two raceways and the outer race with a spherical raceway. Its curvature center of the outer race is consistent with the bearing center, so it has the same centering function as the automatic centering ball bearing. It can be adjusted automatically when the shaft and housing deflect, and this process will not increase the bearing burden. Self-aligning ball bearing ball bearings can bear the loads in two directions, which are radial and axial. Compared with the axial bearing capacity, the self-aligning ball bearing has a greater radial bearing capacity, so it can well deal with heavy load and impact load. The self-aligning ball bearing belongs to the bearing that has tapered holes in the inner diameter of the inner race. It can be installed directly or installed on the cylindrical shaft with a remove pipe or fastening sleeve. The cage is stamped with a steel plate and formed with polyamide. Due to its strong ability to bear heavy load and impact load, self-aligning ball bearings are used in sugar pressing, papermaking, precision instrument, petroleum, cement, metallurgy, mines, low noise motor, motorcycle, rolling mill, automobile, and such industries. Therefore, as such a widely used, fine, and important component, bearing fault diagnosis is a subject that needs to be studied carefully [4–6].

Due to the nonlinear stiffness and bearing clearance of rolling bearing [7, 8], the vibration signal generated by its operation often shows nonstationary and nonlinear. Therefore, extracting useful fault feature information from nonstationary and nonlinear signals is the focus and difficulty of rolling bearing fault diagnosis. Aiming at the problem of bearing fault, many scholars have done lots of research on the early diagnosis of bearing fault [9, 10].

Many scholars apply the methods commonly used in signal processing to bearing fault diagnosis. Many methods of nonlinear dynamic are proposed [11], such as fuzzy

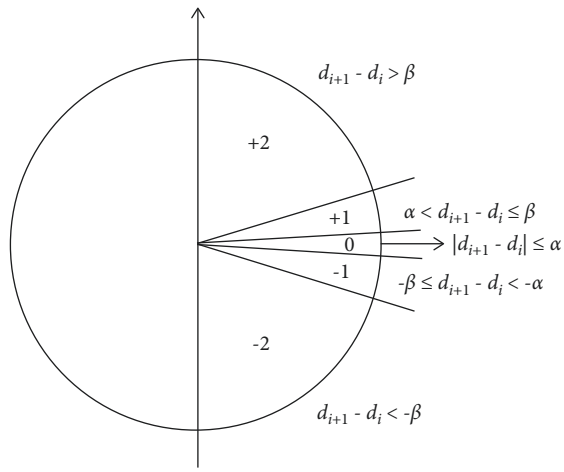

Figure 1: Symbol allotment of SloE.

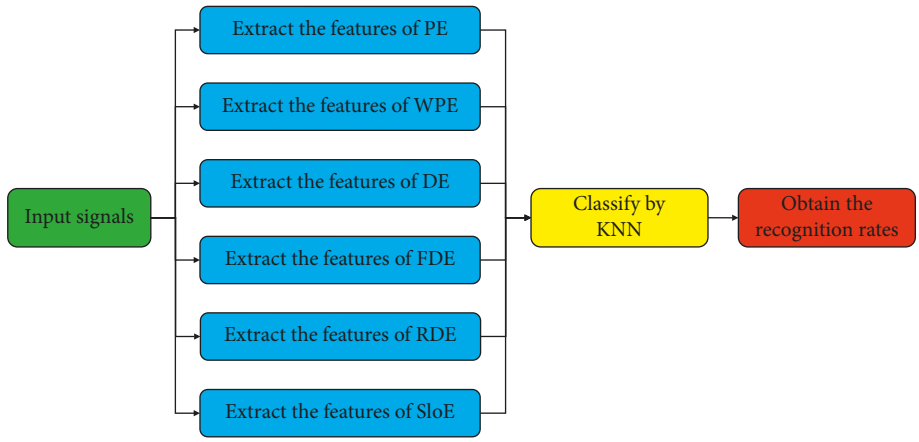

Figure 2: The flow chart of the single feature extraction method.

entropy (FE) [12], permutation entropy (PE) [13], Rényi entropy (RE) [14], dispersion entropy (DE) [15], sample entropy (SE) [16], Wiener entropy (WE) [17], and instantaneous spectral entropy (ISE) [18], which can extract the nonlinear feature of the signals and characterize the health state of the equipment. For SE, its calculation time is long, real-time performance is poor, and similarity measurement is prone to mutation [19]. PE has the advantage of simple calculation, but it ignores the amplitude information of dynamic number sequences [20–25]. Although FE is obtained by improving SE, it still has the disadvantages of slow calculation speed and so on [26–28]. DE has the advantages of small influence by burst signals and better stability, which make up for the problem of PE [29–32]. WE is very sensitive to small alterations. ISE has the relatively low computational burden and fast execution time. Reverse dispersion entropy (RDE) [33] as an improved version of DE has the advantages of both PE and DE and has stronger stability and noise robustness [34, 35]. Similarly, FDE [36] is also an improved version of DE [37], and WPE [38] is an improved version of PE [39, 40]. There are also many other kinds of entropy that are not listed here [41–44].

Slope entropy (SloE) [45] is a new entropy estimator proposed in recent years, which is based on only the vibration amplitude of dynamic number sequences and five symbol patterns. In the three years since it came out, it has been used in many fields, such as medicine and underwater acoustic signal, and achieved excellent results. SloE is applied to the field of medicine by David Cuesta-Frau in 2020 [46, 47], and it is applied to the underwater acoustic signal processing field by Li et al. in 2021 [48]. SloE has a good feature extraction effect in various fields, so it is introduced into the field of fault diagnosis for the first time in this paper.

SloE is applied to the field of bearing fault diagnosis for the first time in this paper. The remaining of the paper is structured as follows: the specific calculation steps of SloE are introduced, and an example of the algorithm is given in Section 2. Section 3 introduces the detailed steps of the experiment and gives a flow chart of the steps. In Section 4, the graphs of the six types of signals are given, the single feature extraction experiment is carried out, and KNN is used for classification. Section 5 is the summary, where the main innovations and conclusions of this paper are given.

2. Slope Entropy

2.1. Basic Principle. SloE is a new algorithm put forward in 2019, which can indicate dynamic number sequence complexity. It is founded on both the vibration amplitude of the

Table 1: Types and codes of the signals.

Type	Normal	Inner race	Ball	Outer race		
				Centered	Orthogonal	Opposite
Code	100	108	121	133	147	160

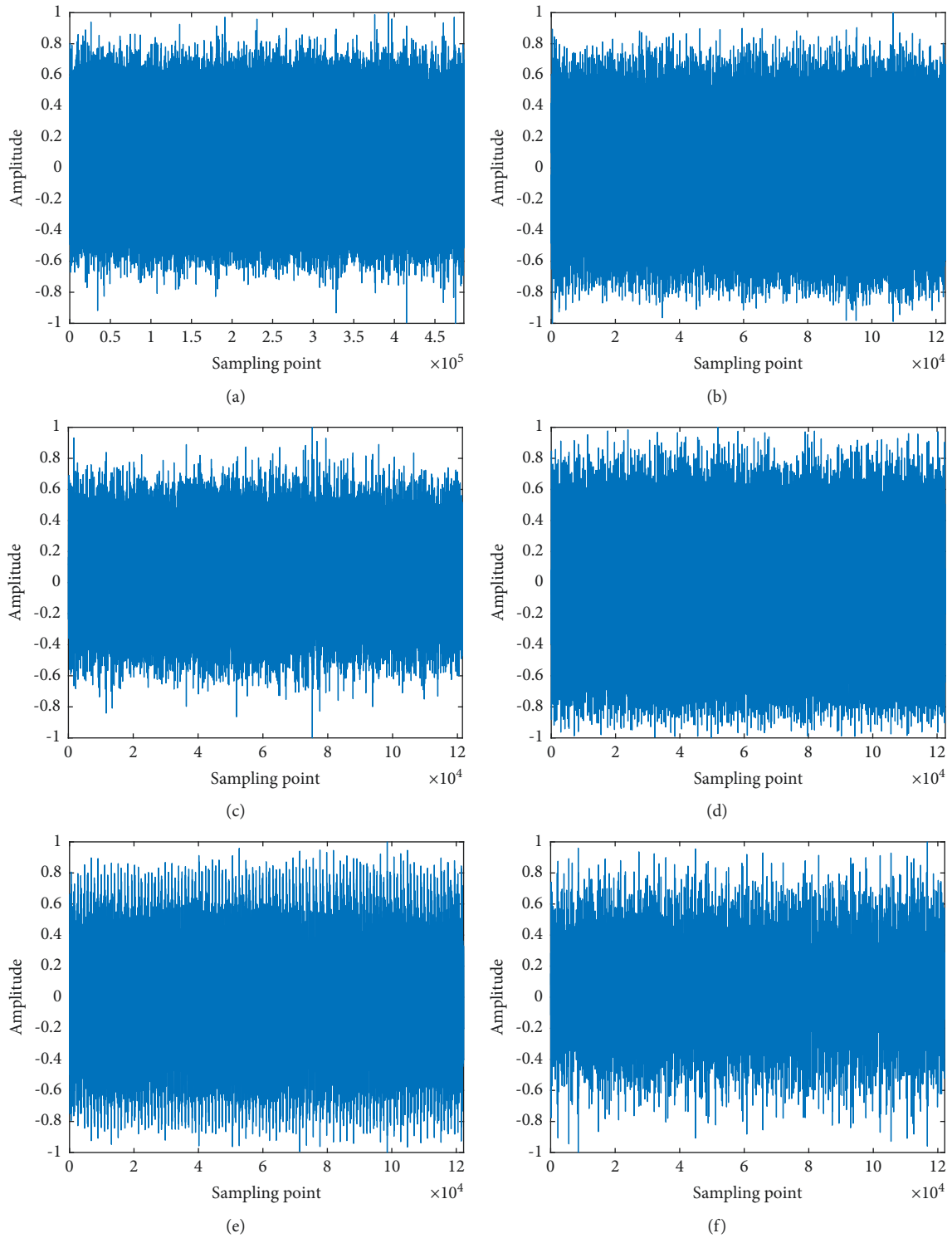

Figure 3: The normalized six types of bearing signals. (a) 100, (b) 108, (c) 121, (d) 133, (e) 147, (f) 160.

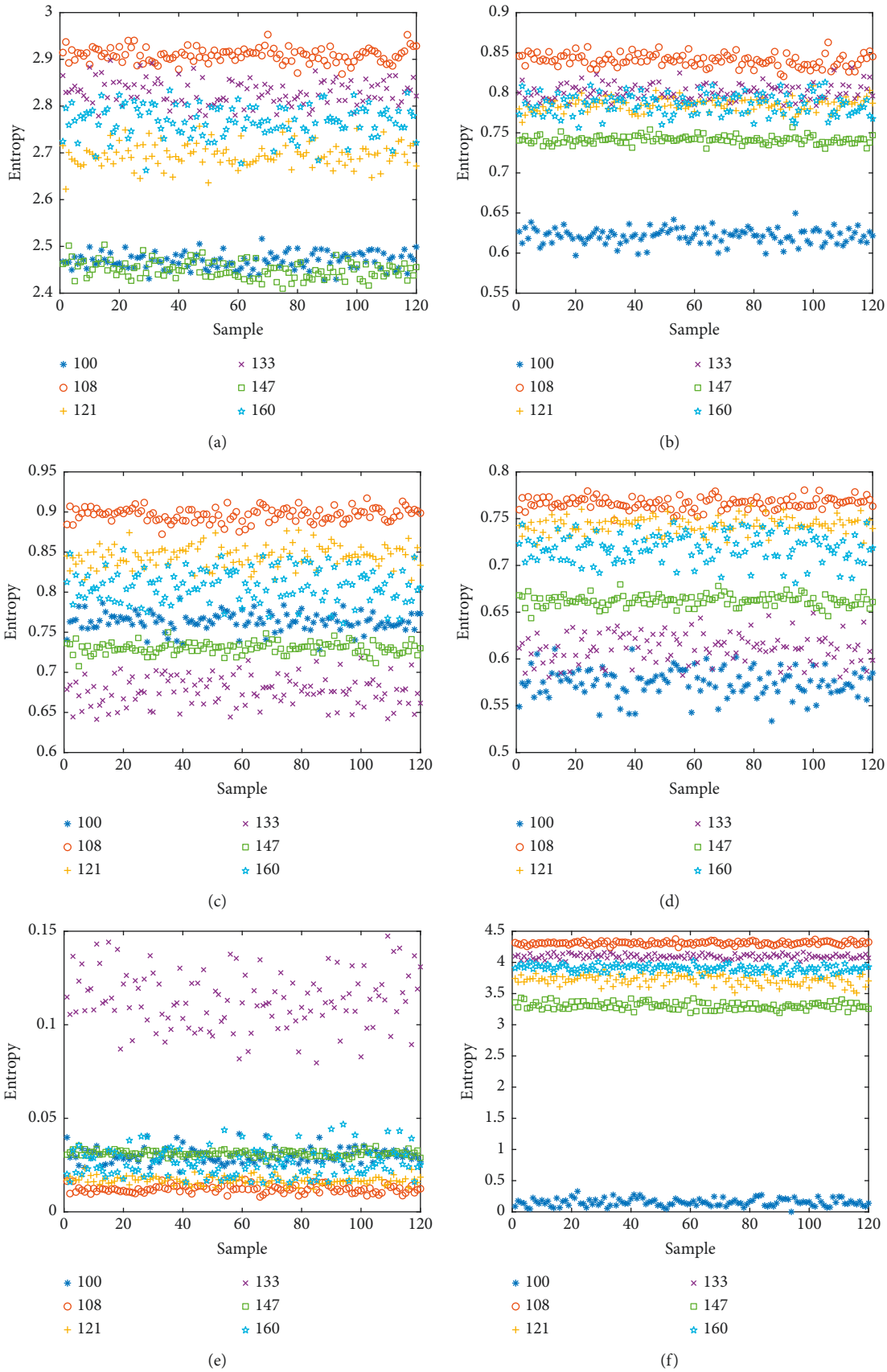

Figure 4: Feature distribution of six types of bearing signals. (a) PE, (b) WPE, (c) DE, (d) FDE, (e) RDE, (f) SlOE.

Table 2: The mean and AMMD of different features.

Entropy	Type	100	108	121	133	147	160
PE	Mean	2.4693	2.9093	2.6961	2.8296	2.4503	2.7676
	AMMD			0.019			
WPE	Mean	0.6214	0.8406	0.7852	0.8016	0.7414	0.7856
	AMMD			0.0004			
DE	Mean	0.7635	0.8968	0.8452	0.6769	0.7302	0.8086
	AMMD			0.0366			
FDE	Mean	0.5751	0.7666	0.7435	0.6117	0.6624	0.7192
	AMMD			0.0231			
RDE	Mean	0.0302	0.0122	0.0169	0.1134	0.0312	0.026
	AMMD			0.001			
SloE	Mean	0.1529	4.3098	3.7154	4.0954	3.3072	3.9055
	AMMD			0.1901			

dynamic number sequence and the five symbol patterns that have been set. Each symbol pattern is allocated according to the difference between the vibration amplitude of the input dynamic number sequences. The calculation process of the SloE algorithm is simple and easy to understand, whose main operation has only addition and subtraction calculations. SloE is calculated as follows.

(1) For given dynamic number sequences $D = \{d_i, i = 1, 2, \ldots, N\}$, the number of subsequences of D is extracted in the light of the embedding dimension m, $D_1 = \{d_1, d_2, \ldots, d_n\}$, $D_2 = \{d_2, d_3, \ldots, d_{n+1}\}$, $\ldots$, $D_k = \{d_k, d_{k+1}, \ldots, d_N\}$, where $k = N - n + 1$.

(2) Diverse symbol modes (+2, +1, 0, −1, −2) are partitioned by the positive and negative values of the two threshold parameters (β and α). Figure 1 is the symbol allotment of SloE.

The specific symbol modes of SloE are assigned in a very unequivocal way. The vertical increments of SloE are decided by β and α, and the horizontal increment between the samples of the continuous dynamic number sequence is always set up as 1. If $\beta = 0.296$, the inclination of the borderlines is 16.5° and −16.5°. And if $\alpha = 0.09$, the boundaries slope of the region of symbol "0" is 5° and -5°.

The specific distribution principles are as follows: if $d_{i+1} - d_i > \beta$, the symbol mode is +2; if $\alpha < d_{i+1} - d_i \le \beta$, the symbol mode is +1; if $|d_{i+1} - d_i| \le \alpha$, the symbol mode is 0; if $-\beta \le d_{i+1} - d_i < -\alpha$, the symbol mode is -1; if $d_{i+1} - d_i < -\beta$, the symbol mode is -2, where $\beta > \alpha > 0$.

(3) Mode sequences $M_1, M_2, \ldots, M_k$, which are corresponding to $D_1, D_2, \ldots, D_k$, are gained after symbol allotment, $M_1 = \{m_1, m_2, \ldots, m_{n-1}\}$, $M_2 = \{m_2, m_3, \ldots, m_n\}$, $\ldots$, $M_k = \{m_k, m_k, \ldots, m_{N-1}\}$, where $k = N - n + 1$, $m_1, m_2, \ldots, m_{N-1}$ are the symbol modes calculated by $d_2 - d_1$, $d_3 - d_2$, $\ldots$, $d_N - d_{N-1}$ through step (2).

(4) Mode sequences have $x = 5^{n-1}$ diverse forms. The quantity of each form is $f_1, f_2, \ldots, f_n$. The frequencies of the mode sequences are the proportions of the number of times they appear: $R_1 = f_1/f$, $R_2 = f_2/f$, $\ldots$, $R_n = f_n/f$. The calculation formula of SloE is defined as follows in view of the classical Shannon entropy:

$$E_s(m) = -\sum_{j=1}^{n} R_j \ln R_j. \quad (1)$$

2.2. Example. Here is a dynamic number sequence $D = \{9, 7, 6, 4, 2, 1, 7, 8, 6, 4, 2, 1, 6, 4, 2, 1\}$, sequence length $N = 16$. Set up the delay time $\varepsilon = 1$, the embedding dimension $m = 4$, and the two threshold parameters $\beta = 1$ and $\alpha = 0.001$. The specific steps of calculating SloE are as follows:

(1) According to D, get the subsequences $D_1 = \{9, 7, 6, 4\}$, $D_2 = \{7, 6, 4, 2\}$, $D_3 = \{6, 4, 2, 1\}$, $D_4 = \{4, 2, 1, 7\}$, $D_5 = \{2, 1, 7, 8\}$, $D_6 = \{1, 7, 8, 6\}$, $D_7 = \{7, 8, 6, 4\}$, $D_8 = \{8, 6, 4, 2\}$, $D_9 = \{6, 4, 2, 1\}$, $D_{10} = \{4, 2, 1, 6\}$, $D_{11} = \{2, 1, 6, 4\}$, $D_{12} = \{1, 6, 4, 2\}$, $D_{13} = \{6, 4, 2, 1\}$.

(2) Then, according to the subsequences, obtain the mode sequences: $M_1 = \{-2, -1, -2\}$, $M_2 = \{-1, -2, -2\}$, $M_3 = \{-2, -2, -1\}$, $M_4 = \{-2, -1, +2\}$, $M_5 = \{-1, +2, +1\}$, $M_6 = \{+2, +1, -2\}$, $M_7 = \{+1, -2, -2\}$, $M_8 = \{-2, -2, -2\}$, $M_9 = \{-2, -2, -1\}$, $M_{10} = \{-2, -1, +2\}$, $M_{11} = \{-1, +2, -2\}$, $M_{12} = \{+2, -2, -2\}$, $M_{13} = \{-2, -2, -1\}$.

(3) There are 10 types of mode sequences. The frequency of $\{-2, -2, -1\}$ is 3, the frequency of $\{-2, -1, +2\}$ is 2, and the frequency of other types is all 1. Therefore, the probabilities are $R_1 = 1/13$, $R_2 = 1/13$, $R_3 = 3/13$, $R_4 = 2/13$, $R_5 = 1/13$, $R_6 = 1/13$, $R_7 = 1/13$, $R_8 = 1/13$, $R_9 = 1/13$, $R_{10} = 1/13$.

(4) Finally, the value of SloE obtained by equation (1) is $E_s(m)$ = -(8 × 1/13 × ln 1/13 + 3/13 × ln 3/13 + 2/13 × ln 2/13) = 2.2048.

3. Proposed Method

A single feature extraction method is put forward for the six types of bearing signals in this experiment. As shown in

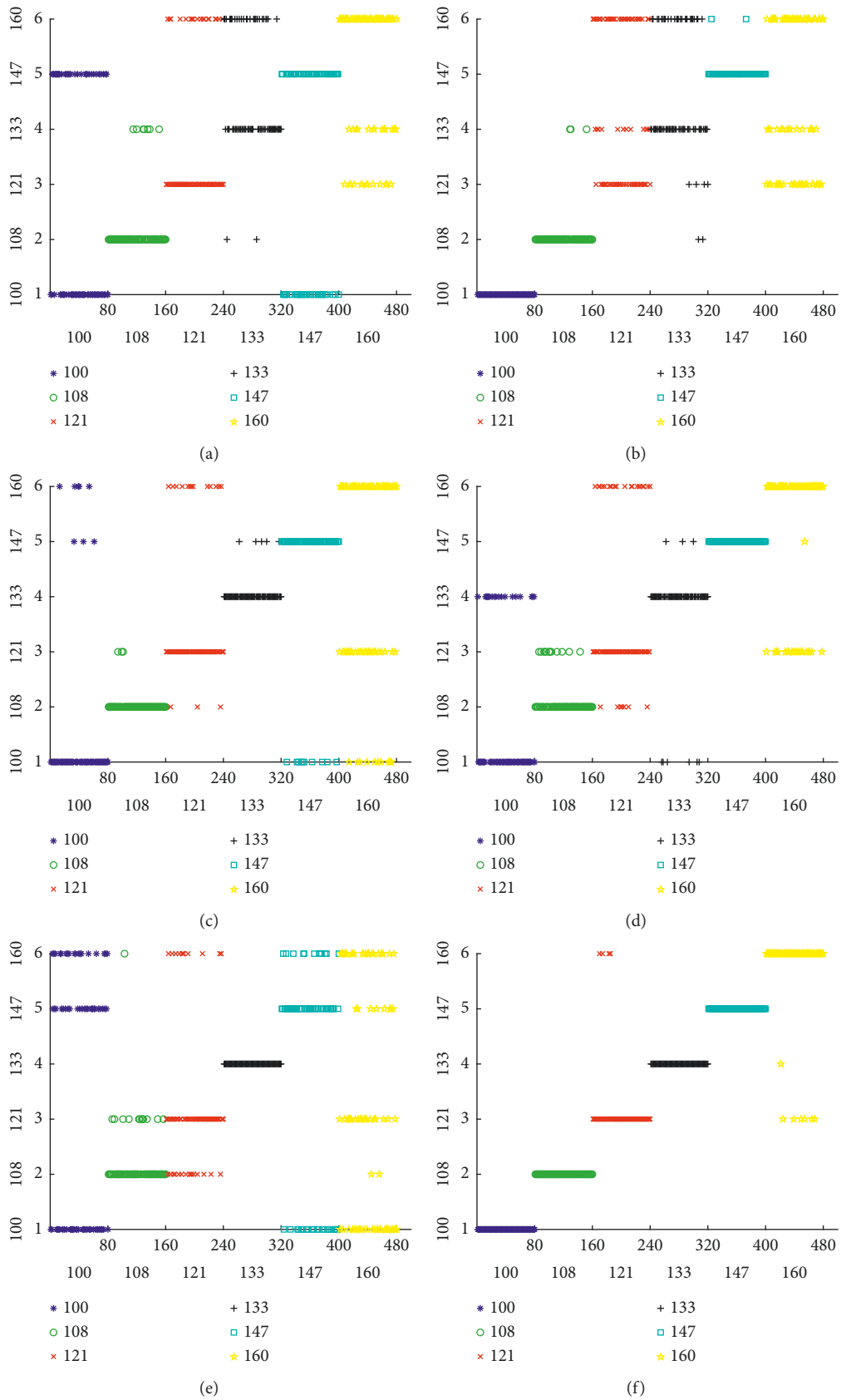

Figure 5: Feature classification and recognition distribution. (a) PE, (b) WPE, (c) DE, (d) FDE, (e) RDE, (f) SLoE.

Table 3: Identification ratios of the feature.

Signals	100 (%)	108 (%)	121 (%)	133 (%)	147 (%)	160 (%)	Average (%)
PE	60	91.25	77.5	63.75	62.5	66.25	70.21
WPE	100	96.25	43.75	58.75	97.5	48.75	74.17
DE	90	96.25	80	93.75	87.5	57.5	84.17
FDE	76.25	85	67.5	88.75	100	72.5	81.67
RDE	47.5	83.75	67.5	100	57.5	30	64.38
SloE	100	100	95	100	100	91.25	97.71

Figure 2 is the flow chart of the single feature extraction method, the particular procedures of the method are as follows.

(1) The six types of bearing signals are imported after being normalized.

(2) For the normal bearing signals or each type of bearing fault signals, which are normalized, 120 samples are selected, where each sample contains 1000 sample points. The features of PE, WPE, DE, FDE, RDE, and SloE are extracted.

(3) K-nearest neighbor (KNN) is chosen as the classifier to classify the features of six kinds of bearing signals. For each type, 40 groups of sample signals are selected as training samples, and 80 groups of sample signals are selected as test samples. The number of nearest samples is set as $k = 3$.

(4) The identification ratios are obtained by operation.

Through these steps, we can conclude that SloE is effective in single-feature classification by comparing the identification ratio calculated by SloE and the others of the five other kinds of entropy.

4. Feature Extraction

4.1. Six Types of Signals. The features of the six types of signals are extracted, which are normal signals, bearing inner race, ball, and outer race fault signals [49]. According to the position relative to the load zone, which is centered, orthogonal, and opposite, there are three types of bearing outer race faults signals. The signals come from the same website, and they are acquired under the same fault diameter, motor load, and motor speed. The names of these signals are replaced by 100, 108, 121, 133, 147, and 160 in the paper. Types and codes of the signals are shown in Table 1.

The lengths of sampling points for them are 485643, 122917, 121556, 122571, 122281, and 122136. The normalized six types of bearing signals are shown in Figure 3.

4.2. Extraction Method. In the feature extraction experiment, for normal signals or each type of bearing fault signal, 120 samples are chosen, and every sample includes 1000 sampling points. These samples almost contain all sampling points of the five bearing fault signals.

For reasonable and scientific comparison, because all kinds of entropy have the same settable parameters the embedding dimension and the delay time, set up them as $m = 4$ and $\varepsilon = 1$. The number of categories is the same settable parameters of DE and two changed versions of DE, set up it as $c = 3$. DE and FDE have the same mapping format, which is the normal cumulative distribution function (NCDF). The two threshold parameters of SloE are set up as $\beta = 0.296$ and $\alpha = 0.09$. Feature distribution of six types of bearing signals is shown in Figure 4.

It can be inferred from Figure 4, for PE distribution, the entropy points of 100 and 147 and the entropy points of 108, 121, 133, and 160 are near to each other; for WPE distribution, almost all entropy points of 121, 133, and 160 are mixed together; for DE and FDE distribution, the entropy points of all types of signals intersect in varying degrees; for RDE distribution, only the entropy points of 133 are significantly distinguished from those of the other five types of signals; for SloE distribution, only a few entropy points of 160 are close to those of 121 and 133. It indicates that SloE has better classification ability on the six types of bearing signals.

For proving the validity of SloE, the mean and the absolute minimum mean difference (AMMD) of diverse features are computed. AMMD is set to the absolute value of the minimum mean difference, and it can intuitively express the distance between the entropy points of the two types of signals, whose entropy points are the closest to each other in the six types of signals. The larger the MMD, the more reliable the interclass separability of the entropy. Table 2 shows the mean and AMMD of different features.

As Table 2 shows, with regard to the six kinds of entropy, the average value of each type of signal has diverse degrees of diversity. RDE has the minimum AMMD of 0.001, and the AMMD of SloE is the maximum, which is 0.1901. It is preliminarily judged that RDE has the worst interclass separability and SloE has the better.

4.3. Feature Classification. For proving the better effect of bearing fault signals feature extraction and classification based on SloE, KNN classification is led into this experiment. For the normal bearing signals or each type of bearing fault signals, which are normalized, 120 samples are selected, where each sample contains 1000 sample points. For each type, 40 groups of sample signals are chosen as training samples, and 80 groups of sample signals are classified as test samples. The feature classification and recognition distribution are shown in Figure 5.

As shown in Figure 5, for these six types of signals, PE and DE have diverse quantities of wrongly classified samples, where the ones of 100 and 160 are separately the largest; WPE, FDE, and RDE only correctly classify the samples of

100, 147, and 133, respectively, but a large number of samples in other signals are classified wrongly; SloE has only a few misclassified samples for 121 and 160, which are classified to 160, 121, and 133, and the other four types of signals are classified correctly; among the six feature extraction methods, 160 has the worst classification effect, while SloE has the best average classification effect. Identification ratios of the feature are shown in Table 3.

As shown in Table 3, for 100, WPE and SloE have the highest classification and identification ratio of 100%, that of DE is 90%, and those of PE, FDE, and RDE are less than 80%; for 108, the classification and identification ratios are more than 90% expect FDE and RDE, where that of SloE is 100%; for 121 and 160, only the classification and C of SloE are more than 90%, and the other kinds of entropy have the classification and identification ratios less than or equal to 80%; for 133, SloE and RDE have the highest classification and identification ratio of 100%, and WPE has the lowest one of 58.75%; for 147, SloE and FDE have the highest classification and identification ratio of 100%, and RDE has the lowest one of 57.5%; for the six types of signals, SloE has the maximum average identification ratio of 97.71%. The mean identification ratios of the other five kinds of entropy are lower than 85%.

The results show that the SloE classification of six kinds of signal samples is the most accurate, and the average identification ratio is the highest.

5. Conclusions

SloE is applied to the field of bearing fault diagnosis, and a new method of extracting features is put forward. The practicability of the proposed method is proved by the feature distribution and the recognition distribution of the six types of measured bearing signals. The main innovations and conclusions are as follows.

(1) SloE is applied to the field of bearing fault diagnosis for the first time.

(2) A new single feature extraction method based on SloE is proposed, and all methods in the paper adopt single feature extraction, which saves a lot of time.

(3) The proposed single feature extraction method based on SloE in this paper has larger AMMD than the single feature extraction method of the six signals based on PE, WPE, DE, FDE, and RDE, which proves that the interclass separability of SloE is better. Moreover, it has the highest average identification ratio of 97.71%, which is higher by at least 13.54% than the others of the other five kinds of entropy.

Data Availability

The data supporting the findings of this study are available within the reference [49].

Conflicts of Interest

The authors declare that they have no conflicts of interest.

References

[1] Z. Chen, A. Mauricio, W. Li, and K. Gryllias, "A deep learning method for bearing fault diagnosis based on cyclic spectral coherence and convolutional neural networks," *Mechanical Systems and Signal Processing*, vol. 140, Article ID 106683, 2020.

[2] K. Kaplan, K. Y. Lmaz, K. Melih, M. N. M. Recep, and E. H. Metin, "An improved feature extraction method using texture analysis with LBP for bearing fault diagnosis," *Applied Soft Computing*, vol. 87, Article ID 106019, 2020.

[3] S. Haidong, C. Junsheng, J. Hongkai, Y. Yu, and W. Zhantao, "Enhanced deep gated recurrent unit and complex wavelet packet energy moment entropy for early fault prognosis of bearing," *Knowledge-Based Systems*, vol. 188, Article ID 105022, 2020.

[4] Y. Li, S. Wang, and Z. Deng, "Intelligent fault identification of rotary machinery using refined composite multi-scale Lempel-Ziv complexity," *Journal of Manufacturing Systems*, vol. 61, pp. 725–735, 2021.

[5] B. Cai, H. Liu, and M. Xie, "A real-time fault diagnosis methodology of complex systems using object-oriented Bayesian networks," *Mechanical Systems and Signal Processing*, vol. 80, pp. 31–44, 2016.

[6] Y. Li, X. Wang, Z. Liu, X. Liang, and S. Si, "The entropy algorithm and its variants in the fault diagnosis of rotating machinery: a review," *IEEE Access*, vol. 6, Article ID 66723, 2018.

[7] T. Han, C. Liu, L. Wu, S. Sarkar, and D. Jiang, "An adaptive spatiotemporal feature learning approach for fault diagnosis in complex systems," *Mechanical Systems and Signal Processing*, vol. 117, pp. 170–187, 2019.

[8] T. Han, Y. Li, and M. Qian, "A hybrid generalization network for intelligent fault diagnosis of rotating machinery under unseen working conditions," *IEEE Transactions on Instrumentation and Measurement*, vol. 70, Article ID 3520011, 2021.

[9] A. Lempel and J. Ziv, "On the complexity of finite sequences," *IEEE Transactions on Information Theory*, vol. 22, no. 1, pp. 75–81, 1976.

[10] Z. Zhang, A. Verma, and A. Kusiak, "Fault analysis and condition monitoring of the wind turbine gearbox," *IEEE Transactions on Energy Conversion*, vol. 27, no. 2, pp. 526–535, 2012.

[11] L. Zhang, J. Lin, and R. Karim, "Adaptive kernel density-based anomaly detection for nonlinear systems," *Knowledge-Based Systems*, vol. 139, pp. 50–63, 2018.

[12] M. Zair, C. Rahmoune, and D. Benazzouz, "Multi-fault diagnosis of rolling bearing using fuzzy entropy of empirical mode decomposition, principal component analysis, and SOM neural network," *Proceedings of the Institution of Mechanical Engineers - Part C: Journal of Mechanical Engineering Science*, vol. 233, no. 9, pp. 3317–3328, 2019.

[13] C. Bandt and B. Pompe, "Permutation entropy: a natural complexity measure for time series," *Physical Review Letters*, vol. 88, Article ID 174102, 2002.

[14] Y. Yin, K. Sun, and S. He, "Multiscale permutation Rényi entropy and its application for EEG signals," *PLoS One*, vol. 13, Article ID 0202558, 2018.

[15] M. Rostaghi and H. Azami, "Dispersion entropy: a measure for time-series analysis," *IEEE Signal Processing Letters*, vol. 23, no. 5, pp. 610–614, 2016.

[16] J. S. Richman and J. R. Moorman, "Physiological time-series analysis using approximate entropy and sample entropy," *American journal of physiology. Am. J. Physiol.-Heart Circ. Physiol*, vol. 6, pp. 2039–2049, 2000.

[17] R. Ceravolo, M. Civera, E. Lenticchia, G. Miraglia, and C. Surace, "Detection and localization of multiple damages through entropy in information theory," *Applied Sciences*, vol. 13, 2021.

[18] M. Civera and C. Surace, "An application of instantaneous spectral entropy for the condition monitoring of wind turbines," *Applied Sciences*, vol. 3, 2022.

[19] Z. Jinde, C. Junsheng, and Y. Yu, "A rolling bearing fault diagnosis approach based on LCD and fuzzy entropy," *Mechanism and Machine Theory*, vol. 70, pp. 441–453, 2013.

[20] L. Tylová, J. Kukal, V. Hubata-Vacek, and O. Vyšata, "Unbiased estimation of permutation entropy in EEG analysis for Alzheimer's disease classification," *Biomedical Signal Processing and Control*, vol. 39, pp. 424–430, 2018.

[21] D. Xie, S. Hong, and C. Yao, "Optimized variational mode decomposition and permutation entropy with their application in feature extraction of ship-radiated noise," *Entropy*, vol. 23, 2021.

[22] C. Bandt, "A new kind of permutation entropy used to classify sleep stages from invisible EEG microstructure," *Entropy*, vol. 19, 2017.

[23] J. Qu, C. Shi, F. Ding, and W. Wang, "A novel aging state recognition method of a viscoelastic sandwich structure based on permutation entropy of dual-tree complex wavelet packet transform and generalized Chebyshev support vector machine," *Structural Health Monitoring*, vol. 19, no. 1, pp. 156–172, 2020.

[24] D. Li, X. Li, Z. Liang, L. J. Voss, and J. W. Sleigh, "Multiscale permutation entropy analysis of EEG recordings during sevoflurane anesthesia," *Journal of Neural Engineering*, vol. 7, Article ID 046010, 2010.

[25] H. Azami and J. Escudero, "Improved multiscale permutation entropy for biomedical signal analysis: interpretation and application to electroencephalogram recordings," *Biomedical Signal Processing and Control*, vol. 23, pp. 28–41, 2016.

[26] Z. Jinde, P. Haiyang, T. Jinyu, and L. Qingyun, *Generalized Refined Composite Multiscale Fuzzy Entropy and Multi-Cluster Feature Selection Based Intelligent Fault Diagnosis of Rolling Bearing*, ISA Trans, Beaumont de, France, 2021.

[27] J. Zheng, J. Cheng, Y. Yang, and S. Luo, "A rolling bearing fault diagnosis method based on multi-scale fuzzy entropy and variable predictive model-based class discrimination," *Mechanism and Machine Theory*, vol. 78, pp. 187–200, 2014.

[28] F. Xu and P. W. Tse, "A method combining refined composite multiscale fuzzy entropy with PSO-SVM for roller bearing fault diagnosis," *Journal of Central South University*, vol. 26, no. 9, pp. 2404–2417, 2019.

[29] J. Zheng and H. Pan, "Use of generalized refined composite multiscale fractional dispersion entropy to diagnose the faults of rolling bearing," *Nonlinear Dynamics*, vol. 101, no. 2, pp. 1417–1440, 2020.

[30] M. Rostaghi, M. R. Ashory, and H. Azami, "Application of dispersion entropy to status characterization of rotary machines," *Journal of Sound and Vibration*, vol. 438, pp. 291–308, 2019.

[31] W. Zhang and J. Zhou, "A comprehensive fault diagnosis method for rolling bearings based on refined composite multiscale dispersion entropy and fast ensemble empirical mode decomposition," *Entropy*, vol. 21, 2019.

[32] H. Azami, M. Rostaghi, D. Abasolo, and J. Escudero, "Refined composite multiscale dispersion entropy and its application to biomedical signals," *IEEE Transactions on Biomedical Engineering*, vol. 64, pp. 2872–2879, 2017.

[33] Y. Li, X. Gao, and L. Wang, "Reverse dispersion entropy: a new complexity measure for sensor signal," *Sensors*, vol. 19, 2019.

[34] Y.-x. Li, S.-b. Jiao, and X. Gao, "A novel signal feature extraction technology based on empirical wavelet transform and reverse dispersion entropy," *Defence Technology*, vol. 17, no. 5, pp. 1625–1635, 2021.

[35] Y. Li, S. Jiao, B. Geng, and Y. Zhou, "Research on feature extraction of ship-radiated noise based on multi-scale reverse dispersion entropy," *Applied Acoustics*, vol. 173, Article ID 107737, 2021.

[36] H. Azami and J. Escudero, "Amplitude- and fluctuation-based dispersion entropy," *Entropy*, vol. 20, 2018.

[37] Z. Li, Y. Li, and K. Zhang, "A feature extraction method of ship-radiated noise based on fluctuation-based dispersion entropy and intrinsic time-scale decomposition," *Entropy*, vol. 21, 2019.

[38] B. Fadlallah, B. Chen, A. Keil, and J. Príncipe, "Weighted-permutation entropy: a complexity measure for time series incorporating amplitude information," *Physical review. E, Statistical, nonlinear, and soft matter physics*, vol. 87, Article ID 022911, 2013.

[39] B. Deng, L. Cai, S. Li et al., "Multivariate multi-scale weighted permutation entropy analysis of EEG complexity for Alzheimer's disease," *Cognitive Neurodynamics*, vol. 11, no. 3, pp. 217–231, 2017.

[40] W. Zhenya, Y. Ligang, C. Gang, and D. Jiaxin, "Modified multiscale weighted permutation entropy and optimized support vector machine method for rolling bearing fault diagnosis with complex signals," *ISA Transactions*, vol. 114, pp. 470–480, 2021.

[41] Y. Li, X. Liang, Y. Wei, and X. Wang, "A method based on refined composite multi-scale symbolic dynamic entropy and ISVM-BT for rotating machinery fault diagnosis," *Neurocomputing*, vol. 315, pp. 246–260, 2018.

[42] Z. Wang, L. Yao, and Y. Cai, "Rolling bearing fault diagnosis using generalized refined composite multiscale sample entropy and optimized support vector machine," *Measurement*, vol. 156, Article ID 107574, 2020.

[43] S. Jiao, B. Geng, and Y. Li, "Fluctuation-based reverse dispersion entropy and its applications to signal classification," *Applied Acoustics*, vol. 175, no. 4, Article ID 107857, 2021.

[44] L. Yongjian, S. Hao, M. Bingrong, Z. Weihua, and X. Qing, "Improved multiscale weighted-dispersion entropy and its application in fault diagnosis of train bearing," *Measurement Science and Technology*, vol. 32, Article ID 075002, 2021.

[45] D. Cuesta-Frau, "Slope entropy: a new time series complexity estimator based on both symbolic patterns and amplitude information," *Entropy*, vol. 21, 2019.

[46] D. Cuesta-Frau, P. H. Dakappa, C. Mahabala, and A. R. Gupta, "Fever time series analysis using slope entropy. Application to early unobtrusive differential diagnosis," *Entropy*, vol. 22, 2020.

[47] D. Cuesta-Frau, J. Schneider, E. Bakštein, P. Vostatek, F. Spaniel, and D. Novák, "Classification of actigraphy records from bipolar disorder patients using slope entropy: a feasibility study," *Entropy*, vol. 22, 2020.

[48] Y. Li, P. Gao, and B. Tang, "Double feature extraction method of ship-radiated noise signal based on slope entropy and permutation entropy," *Entropy*, vol. 24, no. 1, 2022.

[49] Case Western Reserve University, "Bearing data center," 2021, https://engineering.case.edu/bearingdatacenter/pages/welcome-case-western-reserve-university-bearing-data-center-website.